Drug Design, Development and Therapy

Dovepress
Taylor & Francis Group

Open Access Full Text Article

ORIGINAL RESEARCH

Diallyl Disulfide Mitigates LPS-Induced Inhibition of Osteogenic Differentiation and Alleviates Inflammatory Bone Loss via PI3K/AKT Signaling Pathway

Jinze Wu[1,*], Debin Guo[2,*], Yimin Du[3,*], Zi Wang[4,*], Shidan Li[1], Honghao Xu[1], Xiang Chu[1], Xiaowen Gao[5], Lei Li[6], Jun Fei[1]

[1]War Trauma Medical Center, State Key Laboratory of Trauma and Chemical Poisoning, Army Medical Center, Daping Hospital, Army Medical University, Chongqing, 400042, People's Republic of China; [2]Department of Emergency, Army Medical Center, Daping Hospital, Army Medical University, Chongqing, 400042, People's Republic of China; [3]Department of Paediatric Oncology, Haematology, Oncology and Immunology, Heidelberg University, Heidelberg, Germany; [4]Department of Orthopedics, Affiliated Hospital of Southwest Medical University, Luzhou, 646000, People's Republic of China; [5]Department of Emergency, The People's Hospital of Nan'an District, Chongqing, 400060, People's Republic of China; [6]Department of Stem Cell and Regenerative Medicine, Army Medical Center, Daping Hospital, Army Medical University, Chongqing, 400042, People's Republic of China

*These authors contributed equally to this work

Correspondence: Lei Li; Jun Fei, War Trauma Medical Center, State Key Laboratory of Trauma and Chemical Poisoning, Army Medical Center, Daping Hospital, Army Medical University, No. 10 Changjiang Branch Road, Yuzhong District, Chongqing, 400042, People's Republic of China, Email leili@cjtrauma.com; feijundoctor@sohu.com

Background: Systemic inflammation impairs bone health by inhibiting the osteogenic differentiation of bone marrow stromal cells (BMSCs), thereby contributing to bone loss. Diallyl disulfide (DADS), a natural compound with anti-inflammatory properties, was investigated for its ability to mitigate inflammatory bone loss (IBL), reverse LPS-induced suppression of osteogenic differentiation, and elucidate the underlying mechanisms.

Methods: An LPS-induced mouse model of IBL was used to evaluate the effects of DADS by micro-CT, histological and immunohistochemical staining, and serum ELISA. An in vitro model was established by exposing BMSCs to LPS. The optimal concentration of DADS was determined using a Cell Counting Kit-8 (CCK-8) assay. Osteogenic differentiation was evaluated by alkaline phosphatase (ALP) staining, Alizarin Red S (ARS) staining, immunofluorescence, and Western blot. Network pharmacology and transcriptome sequencing were employed to identify potential therapeutic mechanisms, and the PI3K/AKT pathway was verified using the inhibitor LY294002.

Results: Micro-CT and histological analyses confirmed that DADS attenuated bone loss in the IBL mouse model. Toluidine blue staining and immunohistochemical analysis demonstrated that DADS promoted osteogenic differentiation. Immunohistochemical detection and serum ELISA of inflammatory cytokines revealed that DADS significantly reduced inflammatory levels in IBL mice. In vitro, the LPS-induced inhibition of osteogenic differentiation in BMSCs was reversed by DADS. Following DADS treatment, elevated ALP activity, matrix mineralization, and osteogenic marker expression, and reducing inflammatory mediators were observed. Network pharmacology and transcriptome sequencing revealed that DADS may exert its effects through the PI3K/AKT signaling pathway. Subsequent experiments conclusively established that DADS activated the PI3K/AKT signaling pathway. The osteogenic differentiation induced by DADS was inhibited by the PI3K inhibitor LY294002, indicating that the PI3K/AKT pathway is crucial in the osteogenic differentiation promoted by DADS.

Conclusion: DADS counteracts LPS-induced bone loss by promoting osteogenic differentiation via PI3K/AKT activation, highlighting its therapeutic potential for inflammatory bone diseases.

Keywords: inflammatory bone loss, diallyl disulfide, PI3K/AKT, osteogenic differentiation

https://doi.org/10.2147/DDDT.S590959
Received: 11 January 2026
Accepted: 9 April 2026
Published: 14 April 2026

Introduction

Inflammatory bone loss (IBL) is a pathological process in which inflammation disrupts the balance between bone resorption and bone formation, resulting in a net loss of bone mass. This condition commonly occurs in many diseases, including rheumatoid arthritis, periodontitis, chronic osteomyelitis, osteoporosis, and inflammatory bowel disease.[1–4] This pathological state is characterized by the elevated production of pro-inflammatory cytokines, including IL-1β, IL-6, and TNF-α,[5,6] which profoundly impair various normal functions of mesenchymal stem cells (MSCs),[7] including their osteogenic potential. Consequently, this suppression of osteoblast differentiation and activity leads to reduced osteogenesis and bone density.[8,9] Lipopolysaccharide (LPS), a potent endotoxin from Gram-negative bacteria, serves as a widely utilized tool to induce inflammation and mimic pathological conditions, including IBL.[10,11] Upon binding to Toll-like receptor 4 (TLR4), LPS triggers downstream signaling pathways, leading to the release of pro-inflammatory cytokines, and thereby exerts broad biological effects.[12,13]

Current therapeutic strategies for bone loss predominantly target either osteoblast-mediated osteogenesis (anabolic agents) or osteoclast-driven bone resorption (antiresorptive medications). Nonetheless, these traditional methods frequently prove inadequate in cases of bone loss caused by inflammation. This shortcoming arises from their inability to properly tackle the intricate signaling pathways related to inflammation that actively disturb bone homeostasis.[1,14,15] Therefore, concentrating only on correcting the imbalance between ossification and resorption might not lead to the best results. Additionally, there are considerable limitations linked to existing treatments. Teriparatide, a PTH analog, boosts bone formation by triggering PTH receptors on osteoblasts, thus improving bone mineral density.[16] Yet, animal research has linked extended use to a heightened risk of developing osteosarcoma.[17,18] Likewise, denosumab and other anti-RANKL antibodies successfully decrease fracture risk but can unexpectedly impede bone formation during the suppression of resorption.[19] In this context, devising new approaches for treating IBL and understanding their specific mechanisms is essential for overcoming the limitations of current treatments.

Diallyl disulfide (DADS) (Figure 1), a bioactive organosulfur compound derived from garlic, exhibits a broad spectrum of pharmacological properties,[20] including anticancer,[21] anti-inflammatory,[22] and antioxidant activities.[23] It has been shown to suppress the production of inflammatory mediators, inhibit the NF-κB signaling pathway, alleviate cellular oxidative stress, and demonstrate therapeutic potential in diseases such as colitis,[24] coronary atherosclerosis,[25] and hepatic dysfunction.[26] Furthermore, DADS can counteract IL-1β/NF-κB–induced impairment of chondrogenesis in human adipose-derived mesenchymal stem cells by reducing reactive oxygen species (ROS) and enhancing antioxidant enzyme activity.[27] In arthritis models, DADS has also demonstrated protective effects against cartilage degradation, suggesting its beneficial role in skeletal disorders.[28] Importantly, our previous study demonstrated that DADS could inhibit osteoclastogenesis via the NF-κB/NFATc1 signaling axis, thereby alleviating LPS-induced osteolysis in a mouse calvarial model.[29] However, in the context of bone remodeling and repair, it is well-known that the balance between osteoblast-mediated bone formation and osteoclast-mediated bone resorption is crucial for maintaining skeletal homeostasis, and therapeutic strategies that solely target excessive bone resorption are often insufficient to fully reverse established bone loss.[1,30] Building upon these findings and theories, this study expands the scope from bone resorption to bone formation. In contrast to previous studies that have primarily focused on DADS' anti-osteoclastic properties, the current investigation aims to validate whether DADS can treat IBL by enhancing osteogenic differentiation and elucidate its underlying mechanisms. The innovation of this study lies in for the first time, demonstrating DADS' protective effects in a systemic inflammatory bone loss model by promoting osteogenesis, and systematically elucidating the central role of the PI3K/AKT signaling pathway in this process, thereby offering a more comprehensive therapeutic strategy for IBL.

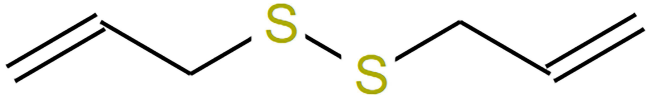

Figure 1 Chemical structure of DADS.

https://doi.org/10.2147/DDDT.S590959

Materials and Methods

LPS-Induced IBL Model and Drug Treatment

30 male C57BL/6 mice (8 weeks old, ~20 g) were purchased from SPF Biotechnology Co., Ltd. (Beijing, China). All mice were housed under standard laboratory conditions (12 h light/dark cycle, 55±2% humidity, 22±2°C) with free access to food and water. An IBL model was induced by LPS (Sigma–Aldrich, Saint Louis, USA) following previously established protocols, and the dose, frequency, and duration (5 mg/kg every 3 days for 3 weeks) were determined based on a comprehensive review of previous studies and preliminary experiments.[31–35] Mice were divided into 5 groups: control, LPS-only (5 mg/kg), LPS + DADS(Sigma–Aldrich, Saint Louis, USA) (20 mg/kg), LPS + DADS (40 mg/kg), and LPS + alendronate sodium (ALN) (10 mg/kg) as a positive control of efficacy, with six mice per group. All groups contained 2% DMSO (Beyotime, Shanghai, China). Except for alendronate sodium, which was administered via oral gavage once a week according to the clinical recommended regimen, the other drugs were administered via intraperitoneal injection every three days. After three weeks, mice were euthanized via intraperitoneal injection of sodium pentobarbital (150 mg/kg). Spleens were collected, weighed, and fixed, and their index was calculated as (spleen weight/body weight) × 100%. Blood samples were stored at −80°C. The right femur and spine were also collected and fixed.

Microcomputed Tomography (μct)

The right femur was preserved in 4% paraformaldehyde solution. The distal segments of the femur were imaged using a VNC-102 x Micro-CT scanner (Pingsheng Medical, Kunshan, China). The 3D reconstruction software Recon was then used to reconstruct the images. Using Avatar data analysis software, the selected region of interest (ROI) was analyzed. It was made sure that uniform selection of the ROI was done for all the samples to obtain the essential parameter values like bone volume fraction (BV/TV), bone surface-to-volume ratio (BS/TV), trabecular number (Tb.N), trabecular thickness (Tb. Th), bone mineral density (BMD), and trabecular separation (Tb.Sp).

Histological and Histomorphometric Analysis

The femurs were decalcified in 10% EDTA at room temperature for 6 weeks after μCT scanning, followed by embedding in paraffin for further histomorphometric analysis. For toluidine blue staining, 7 μm-thick sections were obtained. Image-Pro Plus 6.0 was used for quantitative assessment of osteoblast surface area to bone surface ratio (Ob.S/BS). For the TRAP staining, 5 μm thick sections were utilized, followed by a quantitative analysis of osteoclast count per unit length of trabeculae (OC.N/B.Pm) as well as osteoclast perimeter/trabecular-perimeter percentage (OC.Pm/Tb.Pm). Moreover, 5 μm-thick sections of the right femurs were also used for H&E staining.

The spine was fixed and preserved in 4% paraformaldehyde solution, followed by paraffin embedding. The 4th lumbar vertebra was sectioned at 5 μm and stained with Von Kossa. The bone area percentage (B. Ar) was measured via Image-Pro Plus 6.0 analysis software.

For quantitative analysis, six random fields of view were captured from the tissue sections of each animal, and the average was calculated to generate a single representative value per animal. These representative values (n = 6 mice per group) were then used for statistical analysis.

Immunohistochemical Staining

The right distal femurs of the mice were decalcified and then subjected to immunohistochemical processing and evaluation. Briefly, femoral sections were equilibrated in 0.1 mol/L Tris buffer for 10 minutes. After blocking with 10% normal goat serum for 1 hour, the sections were subsequently incubated overnight at 4°C with specific primary antibodies diluted against COL1A1 (Abcam, Cambridge, UK), RUNX2 (Cell Signaling Technology, Danvers, MA, USA), IL-6 (Affinity, Jiangsu, China), and TNF-α (Cell Signaling Technology, Danvers, MA, USA), following the dilution instructions provided by the reagent supplier. After the femoral sections were washed with phosphate-buffered saline (PBS), they were incubated with horseradish peroxidase (HRP)-conjugated secondary antibodies (dilution 1:500, ServiceBio, China) at room temperature for 1 hour. The sections were developed via 3,3′-diaminobenzidine (DAB).

Positive staining was determined and graded on the basis of hue, saturation, and intensity (HSI) via the image analysis software Aipathwell (Servicebio, China), and then, H score was calculated.

For quantitative analysis, six random fields of view were captured from the tissue sections of each animal, and the average was calculated to generate a single representative value per animal. These representative values (n = 6 mice per group) were then used for statistical analysis.

Enzyme-Linked Immunosorbent Assay (ELISA)

Serum levels of IL-6, IL-1β, and TNF-α were measured by ELISA using commercial kits (Animalunion Biotechnology, Shanghai, China) following the manufacturer's instructions. Standards or test samples were added to the reaction plates, mixed, and incubated at 37 °C for 50 min. Plates were washed three times and blotted dry. Biotinylated antibody diluent was added to blank wells, and 1× biotinylated antibody working solution to other wells, followed by mixing and incubation at 37 °C for another 50 min. After washing, streptavidin–biotin complex (SABC) working solution was added, mixed, and incubated at 37 °C for 30 min. Plates were washed four times, then TMB substrate was added and incubated in the dark at room temperature for 20 min. Stop solution was added and mixed; absorbance at 450 nm was read within 30 min using a microplate reader.

Culture and Identification of BMSCs

The expansion of human BMSCs (Fumei Biotech, Chongqing, China) adhered to a previously established protocol.[36] The cells were cultured in growth medium supplemented with 1% penicillin–streptomycin (Rockville, MD, USA) in a humidified 37°C incubator with 5% CO_2. The medium was changed every 48 hours, and the cells were passaged at 80% confluence. After expansion to the third passage, flow cytometry confirmed the expression of the surface markers CD34, CD45, CD73, and CD105. BMSCs from passages 3 to 5 were used for further experiments.

Cell Viability Assay

BMSCs (3000 cells/well) were seeded in 96-well plates and cultured overnight at 37°C with 5% CO_2. The following day, the cells were incubated with different concentrations of DADS for 24, 72, or 168 hours. Cell viability was assessed via a Cell Counting Kit-8 (Beyotime, Shanghai, China) according to the manufacturer's instructions. Briefly, the culture medium was removed, and fresh medium containing 10% (v/v) CCK-8 reagent was added to each well, followed by further incubation for 2 hours. The absorbance at 450 nm was measured via a microplate reader (Synergy H4; BioTek Instruments, Winooski, VT, USA) to determine the optimal concentration. Each experiment was independently repeated five times to ensure result reliability.

Osteogenic Differentiation Induction and Drug Treatment of BMSCs

BMSCs were seeded at a density of 10^5 cells per well into the 6-well plates or at 40,000 cells per well into the 12-well plates using the growth medium (Fumei Biotechnology, Chongqing, China). After the cells attained approximately 70–80% confluence, the medium was replaced with an osteogenic induction medium (Sperikon, Sichuan, China) containing 0.1 μmol/l dexamethasone, 10 mmol/l β-glycerophosphate, and 50 μg/mL ascorbic acid. When used in an experiment on cells, the DMSO concentration was kept at 0.04%. The medium was refreshed every 2 days.

The cells were divided into the following groups: control group, LPS group, LPS+DADS low-dose group, and LPS +DADS high-dose group. The control group underwent conventional cell culture for osteogenic induction; the LPS group received additional 10 μg/mL LPS on the basis of the control group; the LPS+DADS low-dose group received additional 25 μg/mL DADS on the basis of the LPS group; and the LPS+DADS high-dose group received additional 50 μg/mL DADS on the basis of the LPS group. Furthermore, when validating the mechanism related to the PI3K/AKT signaling pathway, 10 μM PI3K inhibitor LY294002 (MedChemExpress, Shanghai, China) was added to the LPS+DADS high-dose group.

ALP Staining and Activity Assay

A BCIP/NBT ALP color development kit (Beyotime, Shanghai, China) was used to perform ALP staining. After 7 days of osteogenic differentiation, cells cultured in 12-well plates were gently washed twice with PBS and then fixed with 4%

paraformaldehyde (1 mL/well) for 25 minutes at room temperature. After fixation, the cells were washed twice with PBS and then incubated with 1 mL of BCIP/NBT solution in the dark at room temperature for half an hour. Upon washing twice with PBS to halt the staining reaction, images were taken with the microscope. An ALP assay kit (Beyotime, Shanghai, China) was used to measure ALP activity according to the manufacturer's instructions. Each experiment was independently repeated five times to ensure result reliability.

Alizarin Red Staining (ARS) and Calcium Quantification

After 14 days of inducing osteogenic differentiation, cells were washed twice with PBS. Subsequently, fixation was performed by applying 1 mL well−equilibrated 4% paraformaldehyde to each well at room temperature for 25 minutes. Following fixation, the cells underwent two washes with PBS. 1 mL of Alizarin Red S (Oricell, Guangzhou, China) was added to the wells, and the cells were incubated at room temperature for 15 minutes. Following the withdrawal of the staining solution, the cells were rinsed with PBS twice. The staining results were observed and captured in photographs. In quantitative analysis, 500μL of 10% cetylpyridinium chloride was mixed into each well. From the resultant mixture, 100μL was transferred to the 96-well plate. A microplate reader was used to determine absorbance at 562 nm. Each experiment was independently repeated five times to ensure result reliability.

Immunofluorescence Staining

Upon being subjected to treatment, the cells were washed three times with cold PBS. After that, they were fixed using 4% paraformaldehyde for half an hour and permeabilized with 0.15% Triton X-100 for 20 minutes at room temperature. The samples were blocked with 5% BSA for one hour, followed by an overnight incubation with the primary antibody at 4°C. After the samples were washed, they were incubated with the secondary antibody in the dark for two hours at room temperature and a DAPI for 15 minutes. The slides were ultimately prepared with an anti-fade medium, while images were captured using a fluorescence microscope (Olympus, APXVIEW APX100, Japan). For quantitative analysis, six randomly fields of view were captured per well and averaged to produce a single representative value. Then these representative values (n = 5 independent biological replicates per group) were used for statistical analysis.

Quantitative Real-Time PCR (qRT–PCR) Analysis

As per the instructions of the manufacturer, total RNA was isolated from cells with the application of the Super-Fast Pure Cell RNA Isolation Kit (Vazyme, Nanjing, China). Then, a Nanodrop spectrophotometer (Thermo Fisher Scientific, Waltham, MA, USA) was used to establish the concentration to confirm the quality and quantity of RNA. The HiScript®II OneStep qRT–PCR SYBR Green Kit (Vazyme, Nanjing, China) was used for reverse transcription of the RNA and quantitative evaluation of cDNA. The real-time RT-PCR was conducted using a Bio-Rad CFX96 system, and data were normalized as per the 2-ΔΔCT method. The sequences for amplification using forward and reverse primers are given in Table 1. Each experiment was independently repeated five times to ensure result reliability.

Western Blot

Cells were lysed in RIPA buffer containing protease and phosphatase inhibitors. Protein concentration was determined using a BCA kit (Beyotime, Shanghai, China). SDS-PAGE gels were prepared with a TGX stain-free fast-cast kit (Bio-Rad, Boston, MA, USA). Proteins were separated by electrophoresis and total protein was detected using a Bio-Rad ChemiDoc MP system. Proteins were then transferred onto PVDF membranes, blocked, and incubated overnight at 4 °C with following primary antibodies: COL1A1, ALP (Abcam, Cambridge, UK), RUNX2, TNF-α, p-AKT, AKT (Cell Signaling Technology, Danvers, MA, USA), IL-6 (Affinity. Jiangsu, China), COX-2, p-PI3K, and PI3K (ABclonal, Wuhan, China). After washing, membranes were incubated with secondary antibodies for 2 h at room temperature. Protein bands were visualized using an ECL kit (ABclonal, Wuhan, China) and imaged with a ChemiDoc MP system. Band intensities were quantified using ImageJ software, with total protein served as a loading control. Each experiment was independently repeated five times to ensure result reliability.

Table 1 Primers Used for PCR Analysis

Gene Name	Sequence (Forward, 5′→ 3′)	Sequence (Reverse, 5′→ 3′)
GAPDH	GGAAGCTTGTCATCAATGGAAATC	TGATGACCCTTTTGGCTCCC
COL1A1	GAGGGCCAAGACGAAGACATC	CAGATCACGTCATCGCACAAC
RUNX2	AGGCAGTTCCCAAGCATTTCATCC	GGCAGGTAGGTGTGGTAGTGAG
ALP	ACTCTCCGAGATGGTGGTGGTG	CGTGGTCAATTCTGCCTCCTTCC
OCN	CCTCACACTCCTCGCCCTATT	CCGATGTGGTCAGCCAACTC
IL-1β	TACCTGTCCTGCGTGTTGAAA	GGTGCTGATGTACCAGTTGGG
IL-6	ATGAGGAGACTTGCCTGGTGAA	CTCTGGCTTGTTCCTCACTACTCTC
TNF-α	GCTGCACTTTGGAGTGATCG	ATGAGGTACAGGCCCTCTGA
PTGS2	GCTCTGGCGTCCTTTGACTACAT	TTGAGTCGCTTGCTGATGAGGT

Network Pharmacology Assay

Targets prediction for DADS was conducted using the tcmsp database (https://www.tcmsp-e.com/), the SwissTargetPrediction database (http://www.swisstargetprediction.ch/), and the HERB database (http://herb.ac.cn/). Retrieve targets related to "inflammatory bone loss" and "osteogenic differentiation" respectively from GeneCards (https://www.genecards.org/) and OMIM (https://www.omim.org/). Targets with a relevance score greater than the median in GeneCards, along with all related targets in OMIM were obtained. After deduplication, import the targets of DADS, IBL, and osteogenic differentiation into the network tool (http://www.bioinformatics.com.cn/) to generate a Venn diagram and obtain the intersecting targets. Upload the intersecting targets to STRING (https://cn.string-db.org/) and use Cytoscape v3.10.0 software to obtain the protein-protein interaction (PPI) network. Perform GO and KEGG enrichment analysis on these targets using the DAVID database (david.ncifcrf.gov), and visualize the results using the online platform (https://www.bioinformatics.com).

RNA Sequencing and Data Processing

BMSCs were assigned to three groups under osteogenic differentiation culture: control (Group A), LPS (10 μg/mL, Group B), and LPS (10 μg/mL) + DADS (50 μg/mL, Group C). RNA was extracted and sequenced by LC-Bio Technology Co., Ltd. (Hangzhou, China). After quality verification (RIN > 7.0) with an Agilent Bioanalyzer 2100, mRNA was enriched with oligo(dT) beads, fragmented, reverse-transcribed into cDNA, and ligated with dual-index adapters for library preparation. Following UDG treatment and PCR amplification, a cDNA library with ~300 bp inserts was constructed and sequenced on the Illumina NovaSeq 6000 platform with PE150 mode. Volcano plots identified significantly differentially expressed genes (DEGs) between Group B vs A and Group C vs B using the criteria $|\log2FC| \geq 1$ and FDR-adjusted p-value (qval) < 0.05. GO and KEGG enrichment analyses were performed on intergroup DEGs to screen key biological processes, cellular components, molecular functions and signaling pathways. Bioinformatic analyses were conducted via OmicStudio tools (https://www.omicstudio.cn/tool).

Statistical Analysis

Statistical analyses were performed using GraphPad Prism 10.4.0 software. All statistical analyses were performed using n = independent biological replicates or independent mice per group. Outliers were defined as data points exceeding 1.5 times the interquartile range (IQR) above the 75th percentile or below the 25th percentile (No outliers were detected according to these criteria, and all data were retained in the present study). Normality of the data was assessed using the Shapiro–Wilk test and Q-Q plots. The Brown–Forsythe test was used to examine homogeneity or equality of variance.

For normally distributed data with homogeneous variance, two-way ANOVA was employed in cell viability assays to assess the main effects of concentration and time as well as their interaction, while one-way ANOVA was used for all other analyses; when the assumption of equal variances was violated, Welch's ANOVA was applied. When conducting post hoc tests, Dunnett's test was used for planned comparisons with the reference group, while Tukey's test was employed for all pairwise comparisons. For non-normally distributed data, the nonparametric Kruskal–Wallis test was performed followed by Dunn's post-hoc test for pairwise comparisons. A p-value < 0.05 was considered statistically significant.

Results

DADS Ameliorates LPS-Induced IBL in Mice

We evaluated the efficacy of DADS in a mouse model of LPS-induced IBL, using alendronate sodium (ALN) as a positive control (Figure 2A).[32] μCT analysis of distal femurs showed that LPS induction severely degraded bone microstructure, reducing trabecular number, thickness, and bone density. These effects were markedly reversed by DADS and ALN treatment (Figure 2B). Quantitative analysis confirmed significant deterioration in BV/TV, BS/TV, Tb. N, Tb. Th, BMD, and Tb.Sp following the LPS challenge, all of which were effectively mitigated by DADS (Figure 2C–H). In alignment with the μCT findings, H&E staining revealed that the LPS-only group showed discontinuous bone trabeculae with reduced thickness and increased trabecular separation, while DADS treatment significantly improved these pathological changes, restoring the continuity and thickness of bone trabeculae (Figure 2I). Additionally, Von Kossa staining of lumbar vertebrae indicated that DADS maintained calcified tissue area (B.Ar) (Figure 2J and K). Collectively, the results demonstrate that DADS alleviates LPS-induced IBL in mice.

DADS Improves Osteogenic Differentiation in LPS-Induced IBL Mouse Model

To further validate the osteogenic-promoting effect of DADS in vivo, we performed toluidine blue staining on femoral sections. A significant decrease in the Ob.S/BS was observed following LPS administration, which was notably reversed by DADS treatment (Figure 3A and B). Additionally, the immunohistochemical analysis of crucial osteogenic markers, RUNX2 and COL1A1, confirmed these observations. Both proteins were expressed at much higher levels in the femurs of the group treated with DADS than in the LPS group (Figure 3C–F). In addition, TRAP staining showed that LPS induction led to heightened osteoclast activity, evidenced by an increase in the ratio of OC.N/B.Pm and OC.Pm/Tb.Pm. Conversely, DADS treatment notably reduced these parameters (Figure 3G–I). In summary, the evidence suggests that DADS markedly improves osteogenic differentiation and, to some degree, curtails osteoclast activity in mice subjected to LPS.

DADS Alleviates LPS-Induced Inflammatory Response in Mice

Spleen indices and serum inflammatory cytokines were measured in mouse groups. The spleen index (Figure 4A) and serum levels of IL-1β, IL-6, and TNF-α (Figure 4B–D) increased markedly in mice that received LPS, and administration of different doses of DADS effectively reduced these parameters, showing anti-inflammatory activity. Furthermore, The DADS treatments significantly lowered IL-6 and TNF-α levels in the femur as revealed through immunohistochemical analysis (Figure 4E–H).

Identification of BMSCs and the Effect of DADS on the Viability of BMSCs

The identification of BMSCs by flow cytometry produced expected results. According to Figure 5A, the cells express CD34 and CD45 at a level of below 0.2%, and express CD73 and CD105 at a level of over 99.4%. All of these indicate that the cells labelled were purified mesenchymal stem cells. To evaluate the effects of DADS on BMSC viability, CCK-8 assays were performed at 1, 3, and 7 days. Two-way ANOVA revealed significant main effects of DADS concentration ($P < 0.001$) and incubation time ($P < 0.001$), as well as a significant concentration × time interaction ($P < 0.001$). Given the significant interaction, Dunnett's post-hoc tests were conducted to compare each concentration against the control (0 μg/mL) at each time points. The results showed that BMSCs viability is unaffected by DADS concentrations of 25 and 50 μg/mL at 1 and 3 days. Higher concentrations, however, reduce viability at these time points. After 7 days, DADS concentrations up to 100 μg/mL demonstrate no adverse effect, while supra-threshold concentrations significantly decrease cell survival. Consequently, DADS concentrations ranging from 0 to 50 μg/mL are deemed safe for BMSC viability (Figure 5B).

DADS Reverses the Inhibition of Osteogenic Differentiation in LPS-Induced BMSCs

According to the results from the assays post-osteogenic induction, the ALP staining and activity (Figure 6A and B) substantially reduced due to LPS in comparison to the control. DADS treatment rescued this in a dose-dependent manner.

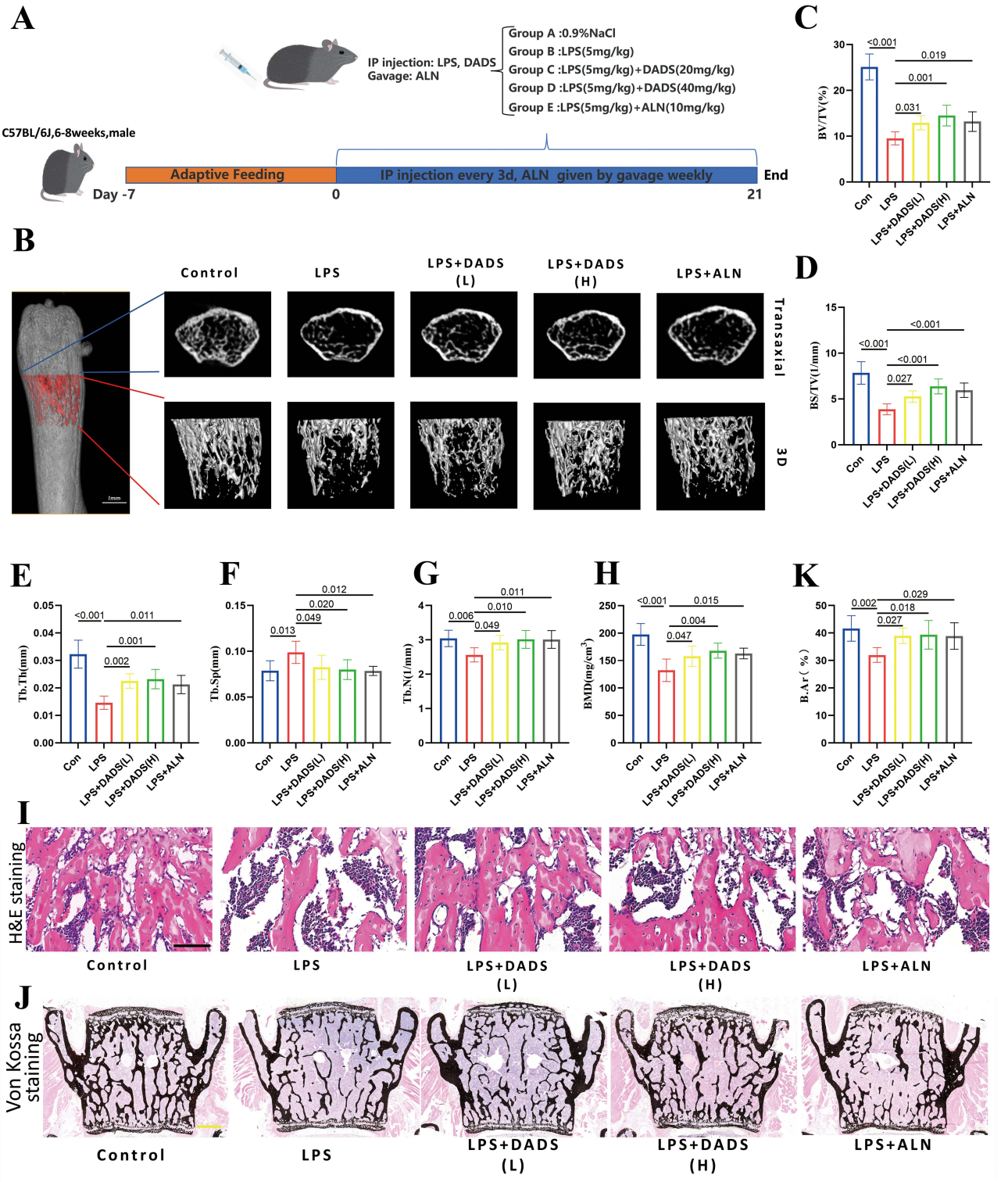

Figure 2 DADS ameliorates LPS-induced IBL in Mice. (**A**) Construction and treatment protocol of the mouse models. (**B**) Representative 3D and transaxial μCT images of mouse distal femurs (scale bar = 1mm). (**C–H**) Quantitative analysis of trabecular bone parameters, including BV/TV, BS/TV, Tb. N, Tb.Th, BMD, and Tb.Sp. (**I**) Representative images of H&E staining showing the structures of distal femur trabecular bone, scale bar = 100 μm. (**J** and **K**) Representative images of Von Kossa-stained bone tissue in the fourth lumbar spine and (**J**) and their quantitative analysis of B.Ar (**K**) (scale bar = 500 μm). Statistical analysis was performed using one-way ANOVA. Data are presented as mean ± SD, n = 6 independent mice per group. Exact P values for pairwise comparisons are shown above the horizontal lines; P < 0.001 denotes values below three-decimal precision.

https://doi.org/10.2147/DDDT.S590959

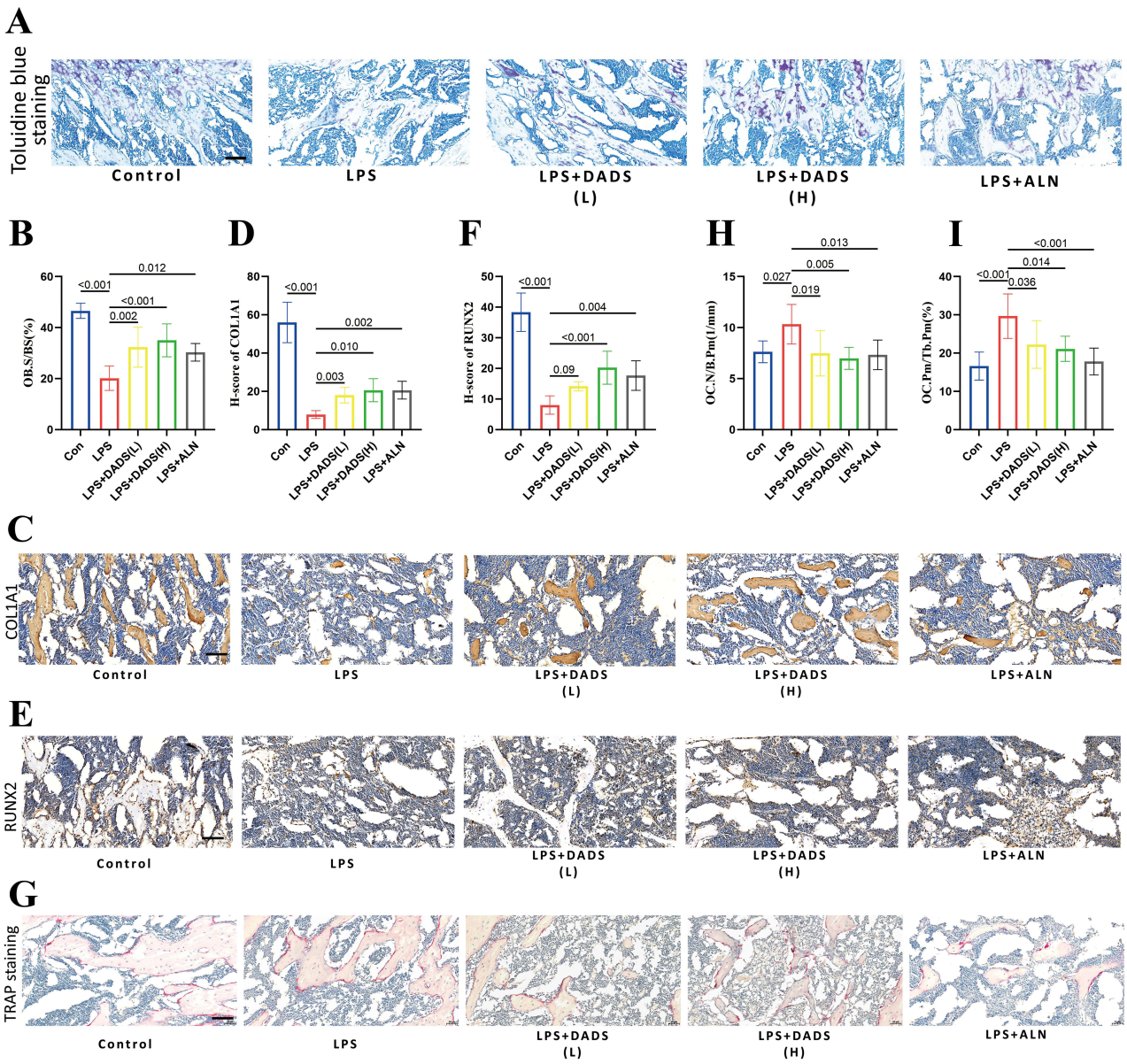

Figure 3 DADS improves osteogenic differentiation in a mouse model of LPS-induced IBL. (**A** and **B**) Representative images of toluidine blue staining of the distal femur (Scale bar =100 μm) (**A**) and quantitative analysis of Ob.S/BS (one-way ANOVA) (**B**). (**C** and **D**) Representative immunohistochemical images of COL1A1 in the distal femur (scale bar = 100 μm) (**C**) and quantitative analysis determined using the H-score method (Welch's ANOVA) (**D**). (**E** and **F**) Representative immunohistochemical images of RUNX2 in the distal femur (**E**) (scale bar = 100 μm) and quantitative analysis determined using the H-score method (one-way ANOVA) (**F**). (**G–I**) Representative images of TRAP staining of osteoclasts in the femurs of the distal femur (scale bar = 100 μm) (**G**) and quantitative analysis of OC.N/B. Pm (**H**) and OC. Pm/Tb. Pm (**I**) (one-way ANOVA). Data are presented as mean ± SD, n = 6 independent mice per group. Exact P values for pairwise comparisons are shown above the horizontal lines; P < 0.001 denotes values below three-decimal precision.

Similarly, the findings of ARS staining and quantification showed LPS reduced calcium deposition, and DADS dose-dependently reinstated this effect (Figure 6C and D). Moreover, according to the outcomes of immunofluorescence staining, the fluorescence densities of RUNX2 and OCN, as osteogenic markers, were increased in DADS-treated groups compared to the LPS-only group (Figure 6E–H). As per qPCR analysis, when LPS is present, DADS increased the expression of osteogenic genes (COL1A1, RUNX2, ALP, and OCN) in a dose-dependent manner (Figure 6I–L). Western blot further confirmed that the quantity of COL1A1 and RUNX2 proteins was significantly increased in LPS+DADS-treated groups compared to the LPS-only group (Figure 6M–O). In total, these data show DADS can reverse the inhibitory effect of LPS on osteogenic differentiation.

https://doi.org/10.2147/DDDT.S590959

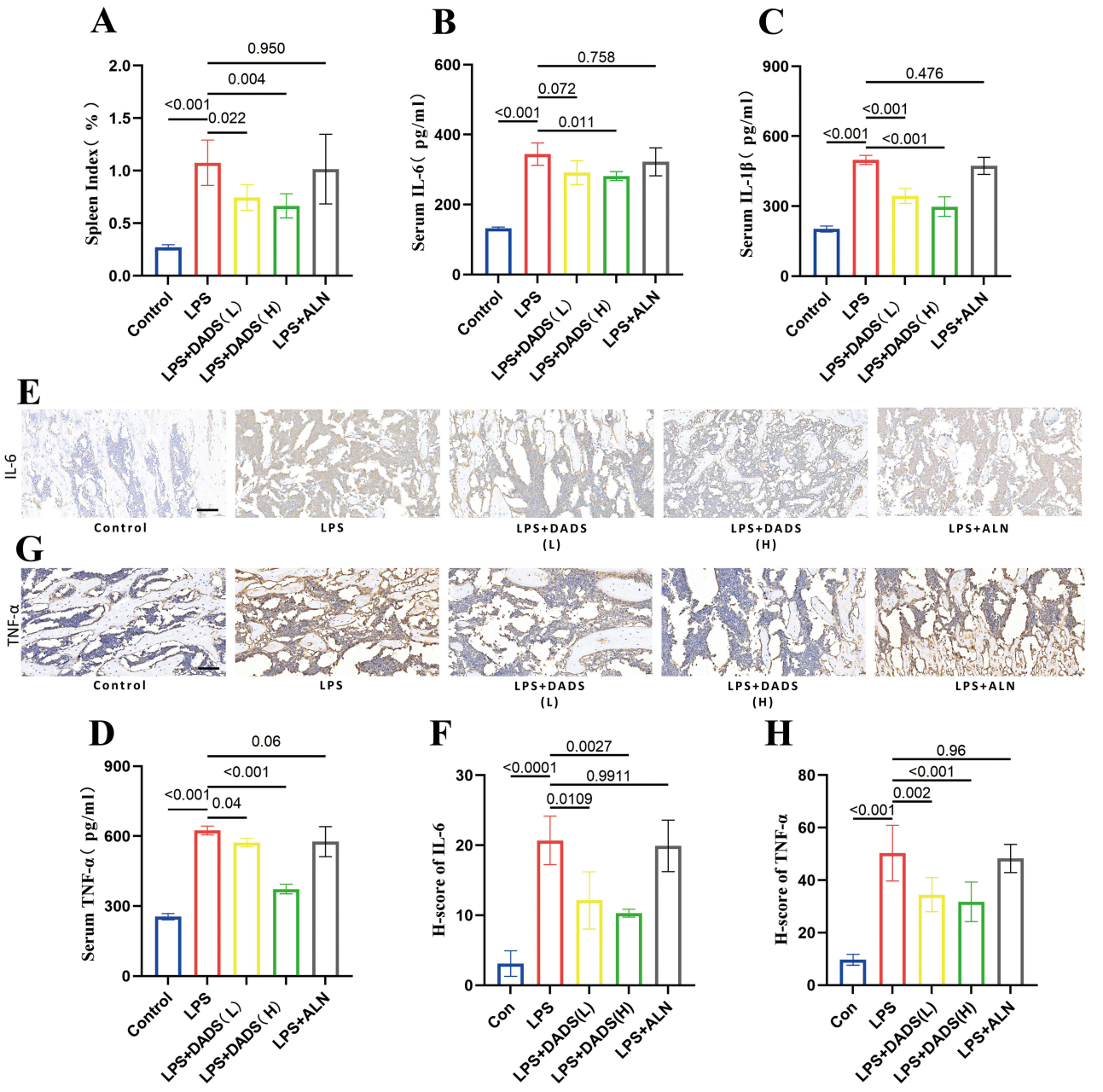

Figure 4 DADS ameliorates LPS-induced inflammatory factors in mice. (**A**) Spleen index (one-way ANOVA). (**B–D**) Measurement of Inflammatory factors in serum, including IL-1β (Welch's ANOVA), IL-6 (Welch's ANOVA), and TNF-α (one-way ANOVA) by ELISA. (**E–H**) Representative immunohistochemical images of IL-6 (**E**) and TNF-α (**G**) proteins in the distal femur (scale bar = 100 μm), along with their quantitative analysis determined using the H-score method (Welch's ANOVA) (**F** and **H**). Data are presented as mean ± SD, n = 6 independent mice per group. Exact P values for pairwise comparisons are shown above the horizontal lines; P < 0.001 denotes values below three-decimal precision.

DADS Downregulates LPS-Induced COX-2 and Inflammatory Cytokines

Three days after the administration of drugs, the mRNA levels of COX-2, IL-1β, IL-6, and TNF-α were elevated with the treatment of LPS, as determined by qPCR. Importantly, Low-dose and high-dose DADS treatment significantly reduced these elevated levels (Figure 7A–D). The result of Western blot analysis verified that COX-2, IL-6, and TNF-α protein levels were reduced by DADS (Figure 7E–J).

https://doi.org/10.2147/DDDT.S590959

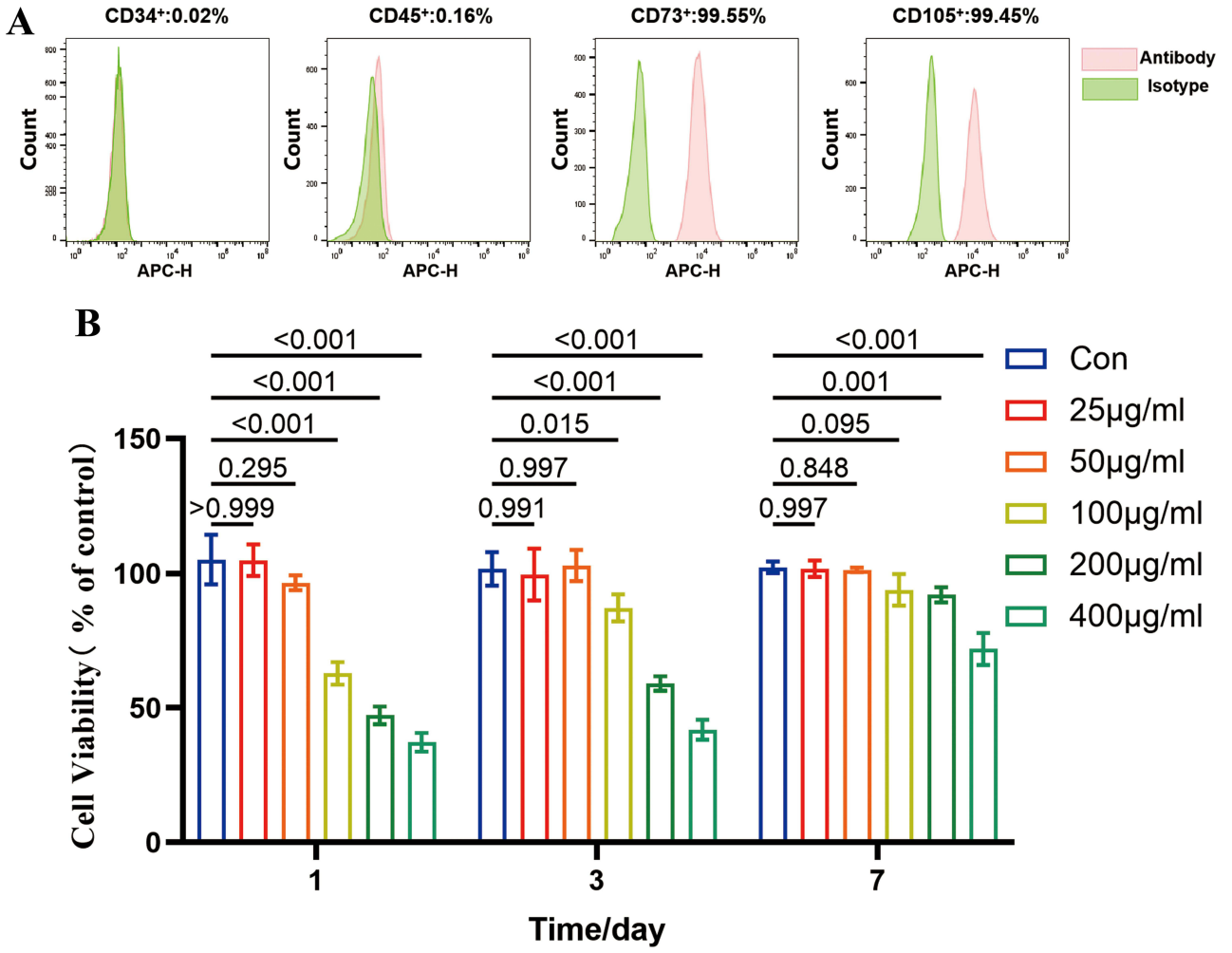

Figure 5 Identification of BMSCs and the effect of DADS on BMSCs' viability. (**A**) CD markers of BMSCs assessed by Flow cytometry. (**B**) Assessment of BMSCs viability after 1, 3, and 7 days of treatment with different concentrations of DADS using the CCK-8 assay (two-way ANOVA). Data are presented as mean ± SD, n = 5 independent biological replicates per group. Exact P values for pairwise comparisons are shown above the horizontal lines; P < 0.001 denotes values below three-decimal precision; P > 0.999 denotes P values above 0.999.

Network Pharmacological Analysis of DADS in Treating IBL by Regulating Osteogenic Differentiation

A sum of 224 DADS-related targets was obtained from the TCMSP, SwissTargetPrediction, and HERB databases. After removing duplicates, 6540 targets of IBL and 1037 genes related to osteogenic differentiation were collected from GeneCards and OMIM, respectively. The intersection of these target sets comprises 34 targets, as represented by the Venn diagram in Figure 8A. Following this, the protein-protein interaction (PPI) network of these 34 targets was constructed through the STRING database and then visualised using Cytoscape v3.10.0 (Figure 8B). We further examined these targets using GO and KEGG pathway enrichment analyses with the DAVID database. According to the GO enrichment analysis, biological processes like response to oxidative stress, ossification, and response to LPS were mostly enriched (Figure 8C–E). The KEGG pathway analysis (Figure 8F) revealed that the TNF and PI3K/AKT signaling pathways were enriched.

https://doi.org/10.2147/DDDT.S590959

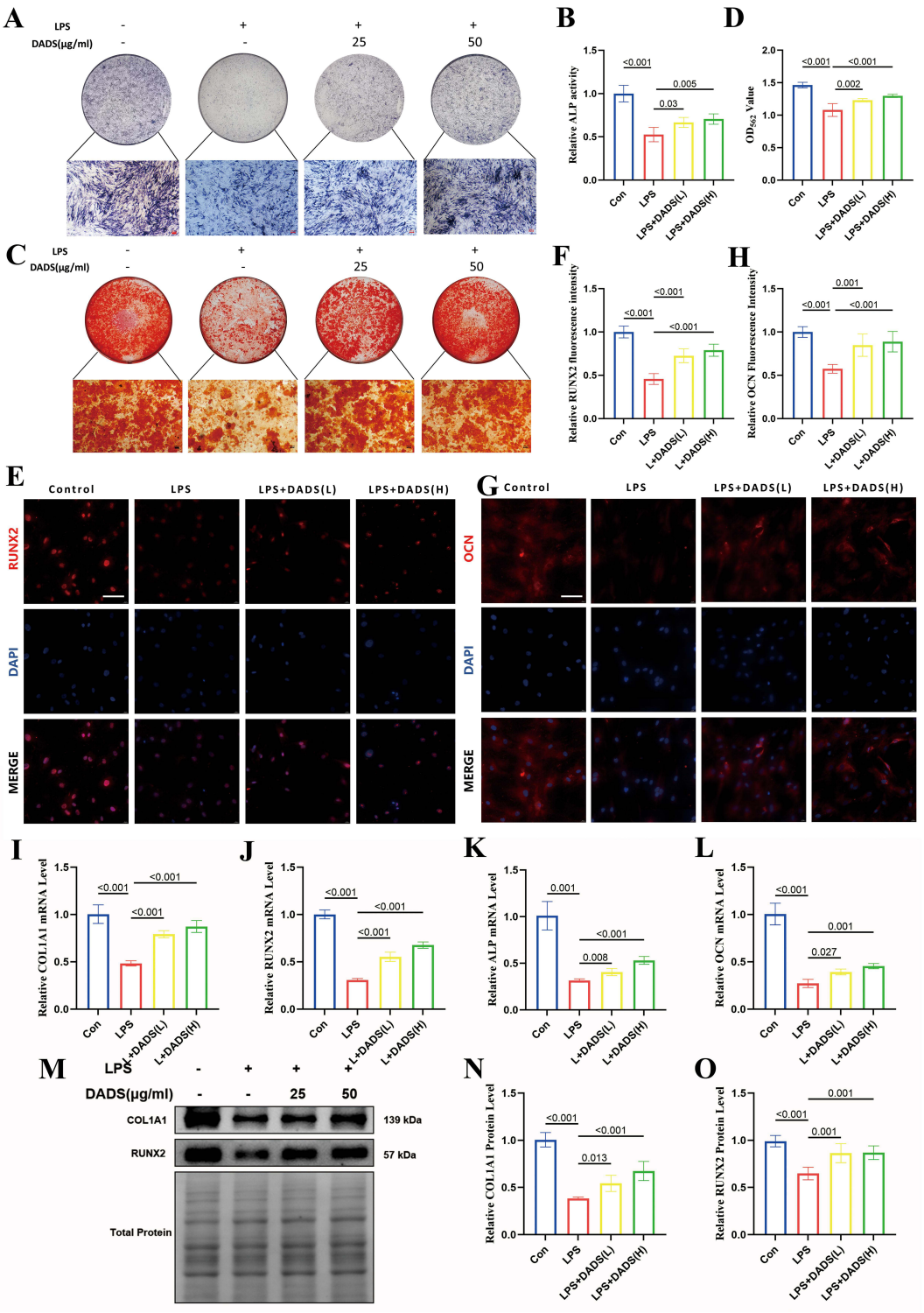

Figure 6 DADS alleviates the inhibition of osteogenic differentiation in LPS-induced BMSCs. (**A**) Representative images of ALP staining after 7 days of osteogenic induction (scale bar = 100 μm). (**B**) ALP activity evaluation (one-way ANOVA). (**C**) Representative images of Alizarin Red staining after 14 days of osteogenic induction (scale bar = 100 μm). (**D**) Quantitative assessment of the calcium deposition in (**C**) (one-way ANOVA). (**E**–**H**) Representative images of immunofluorescence staining for osteogenic markers RUNX2 (**E**) and OCN (**G**) after 7 days of osteogenic induction (scale bar=100 μm), along with their quantitative analysis (one-way ANOVA) (**F** and **H**). (**I**–**L**) The expression of osteogenic-specific genes COL1A1 (one-way ANOVA) (**I**), RUNX2 (one-way ANOVA) (**J**), ALP (Welch's ANOVA) (**K**), and OCN (one-way ANOVA) (**L**) after 7 days of osteogenic induction. (**M**–**O**) Western blot and quantitative analysis of the levels of osteogenic markers COL1A1 and RUNX2 after 7 days of osteogenic induction (one-way ANOVA), with total protein serving as a loading control. Data are presented as mean ± SD, n = 5 independent biological replicates per group. Exact P values for pairwise comparisons are shown above the horizontal lines; P < 0.001 denotes values below three-decimal precision.

https://doi.org/10.2147/DDDT.S590959

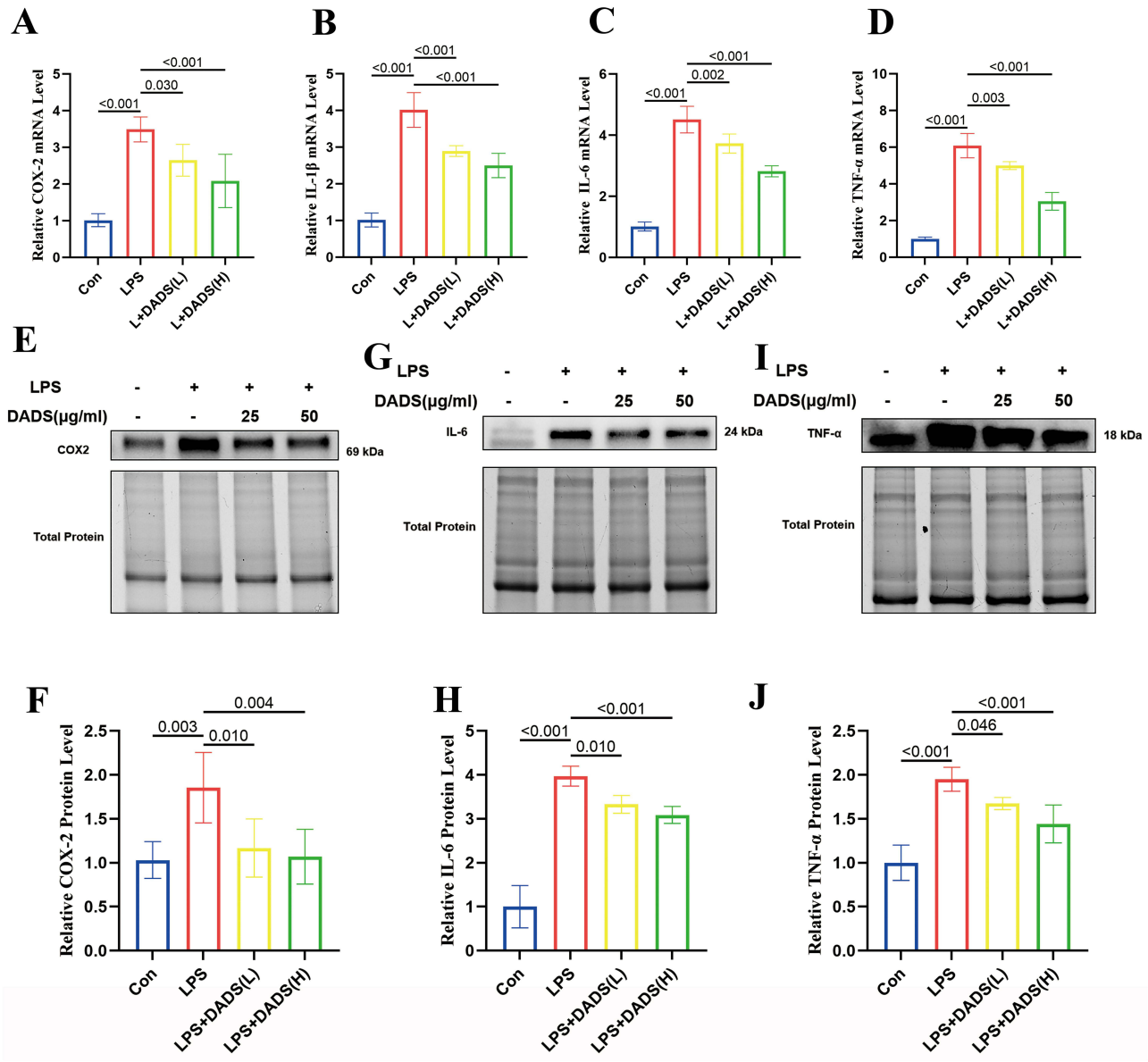

Figure 7 DADS downregulated LPS-induced COX2 and inflammatory factors in BMSCs. (**A**–**D**) qPCR results of PTGS2, IL-1β, IL-6, and TNF-α under different treatment conditions. (**E** and **F**) Representative images of Western blot results for COX-2 and their quantification, with total protein serving as a loading control. (**G**–**J**) Representative images of Western blot results for pro-inflammatory cytokines IL-6 and TNF-α and their quantitative analysis, with total protein serving as a loading control. Statistical analysis was performed using one-way ANOVA. Data are presented as mean ± SD, n = 5 independent biological replicates per group. Exact P values for pairwise comparisons are shown above the horizontal lines; P < 0.001 denotes values below three-decimal precision.

Transcriptome Sequencing Analysis Elucidated the Mechanism of Action of DADS

Principal component analysis (PCA) demonstrated strong intra-group consistency and significant inter-group differences among the three experimental groups (Figure 9A). Volcano plots and hierarchical clustering heatmaps identified 1654 DEGs in the LPS (group B) vs the Control (group A), with 1088 upregulated and 566 downregulated genes. The LPS + DADS (group C) vs the LPS group had 362 DEGs, with 150 upregulated and 212 downregulated (Figure 9B–E). GO enrichment analysis of DEGs for the LPS vs Con group indicated significant differences such as inflammatory response, response to LPS, and cytokine activity (Figure 9F). And for the LPS + DADS vs LPS group, significant enrichment was observed in processes including calcium ion binding, action potential, and glycine cleavage complex (Figure 9G). Notably, in the KEGG enrichment analysis, the PI3K/AKT pathway was significantly enriched in both comparative groups (Figure 9H and I), suggesting its regulation during LPS and DADS intervention.

https://doi.org/10.2147/DDDT.S590959

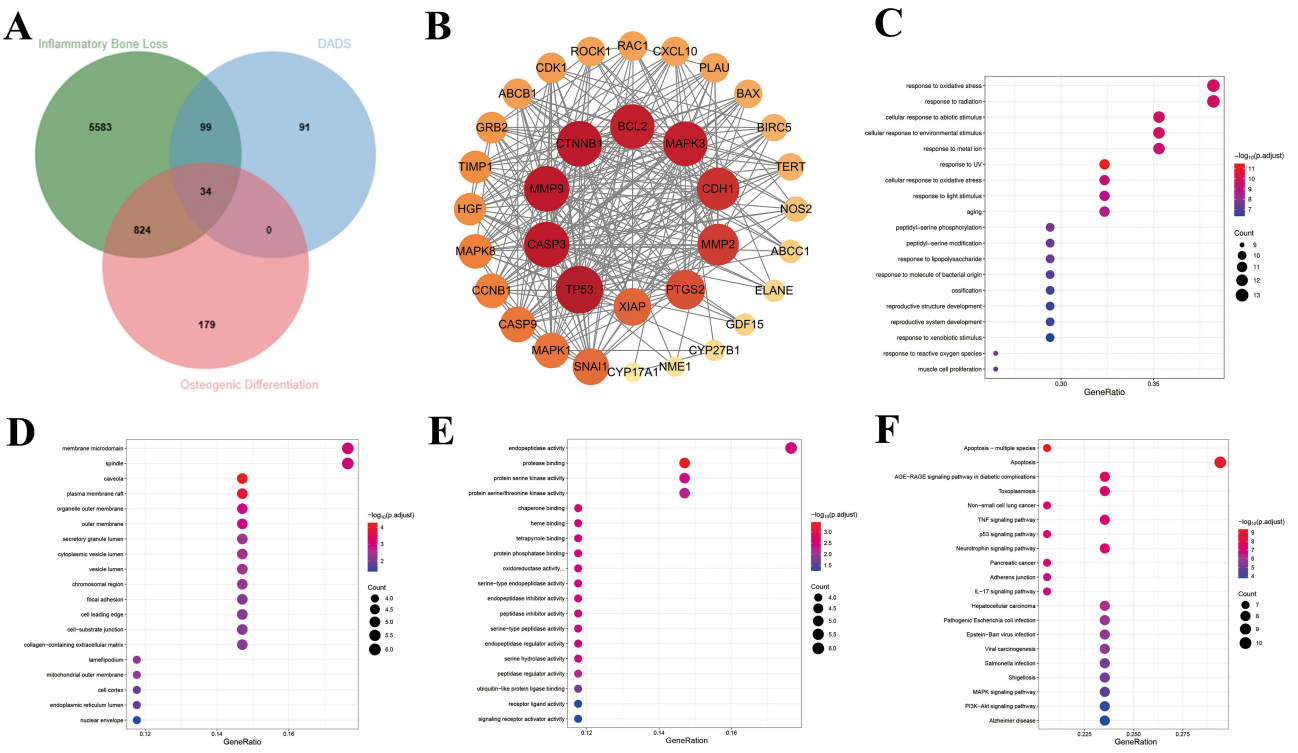

Figure 8 Network pharmacological analysis of DADS in treating IBL by regulating osteogenic differentiation. (**A**) Venn diagram illustrating the intersection of DADS targets with those related to IBL and osteogenic differentiation. (**B**) Protein-protein interaction (PPI) network of the 34 overlapping targets. (**C**–**E**) Gene Ontology (GO) enrichment analysis of the 34 overlapping targets, categorized into Biological Process (BP) (**C**), Cellular Component (CC) (**D**), and Molecular Function (MF) (**E**). (**F**) Kyoto Encyclopedia of Genes and Genomes (KEGG) pathway enrichment analysis of the 34 overlapping targets.

DADS Activates the PI3K/AKT Signaling Pathway

Western blot analysis was used to detect the levels of essential components of the PI3K/AKT pathway. According to the findings, the LPS-treated group showed lower levels of PI3K and AKT phosphorylation (activation markers) compared to the control group. In contrast, treatment with different dosages of DADS successfully reversed this decline (Figure 10A–D), suggesting that activation of the PI3K/AKT signaling pathway is essential for the therapeutic function of DADS.

LY294002 Counteracts the Pro-Osteogenic Differentiation Efficacy of DADS

To investigate whether DADS rescues LPS-induced suppression of osteogenic differentiation by activating the PI3K/AKT signaling pathway, we used the PI3K inhibitor LY294002 to block this pathway. After 7 days of cell treatment, the DADS-induced enhancement of ALP staining and activity was significantly reduced by LY294002 (Figure 11A and B). After 14 days of cell treatment, ARS staining and quantitative analysis also demonstrated that LY294002 significantly inhibited cell mineralization effects (Figure 11C and D). In addition, the application of LY294002 counteracted the upregulation of vital osteogenic genes induced by DADS at the transcriptional level, as evidenced by the expression levels of COL1A1, RUNX2, ALP, and OCN (Figure 11E–H). Moreover, Western blot analysis indicated that LY294002 significantly weakened the effects of DADS on the expression of COL1A1 and RUNX2 proteins (Figure 11I–K). This evidence suggests that the PI3K/AKT signaling pathway plays a critical role in DADS-mediated enhancement of osteogenic differentiation.

 https://doi.org/10.2147/DDDT.S590959

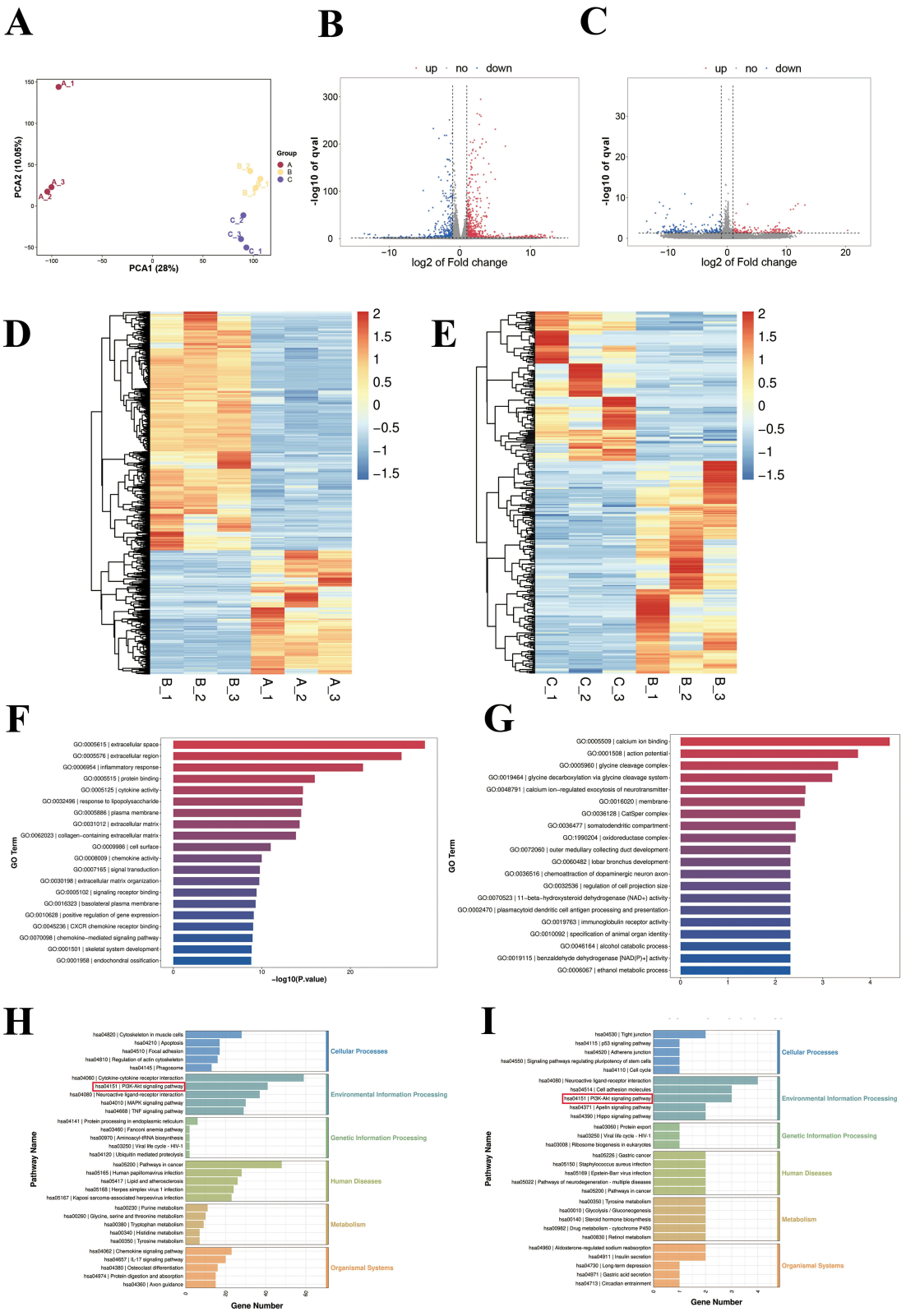

Figure 9 Transcriptome sequencing analysis of Control (Group A), LPS (Group B), and LPS + DADS (Group C). (**A**) PCA analysis among different groups. (**B**) Volcano plot of DEGs in group B vs group A. (**C**) Volcano plot of DEGs in group C vs group B. (**D**) Hierarchical clustering heatmap of DEGs in group B vs group A. (**E**) Hierarchical clustering heatmap of DEGs in group C vs group B. (**F**) GO enrichment analysis of DEGs in group B vs group A. (**G**) GO enrichment analysis of DEGs in group C vs group B. (**H**) KEGG enrichment analysis of DEGs in group B vs group A. (**I**) KEGG enrichment analysis of DEGs in group C vs group B. Red marked box indicates the pathway selected for follow-up experimental validation.

https://doi.org/10.2147/DDDT.S590959

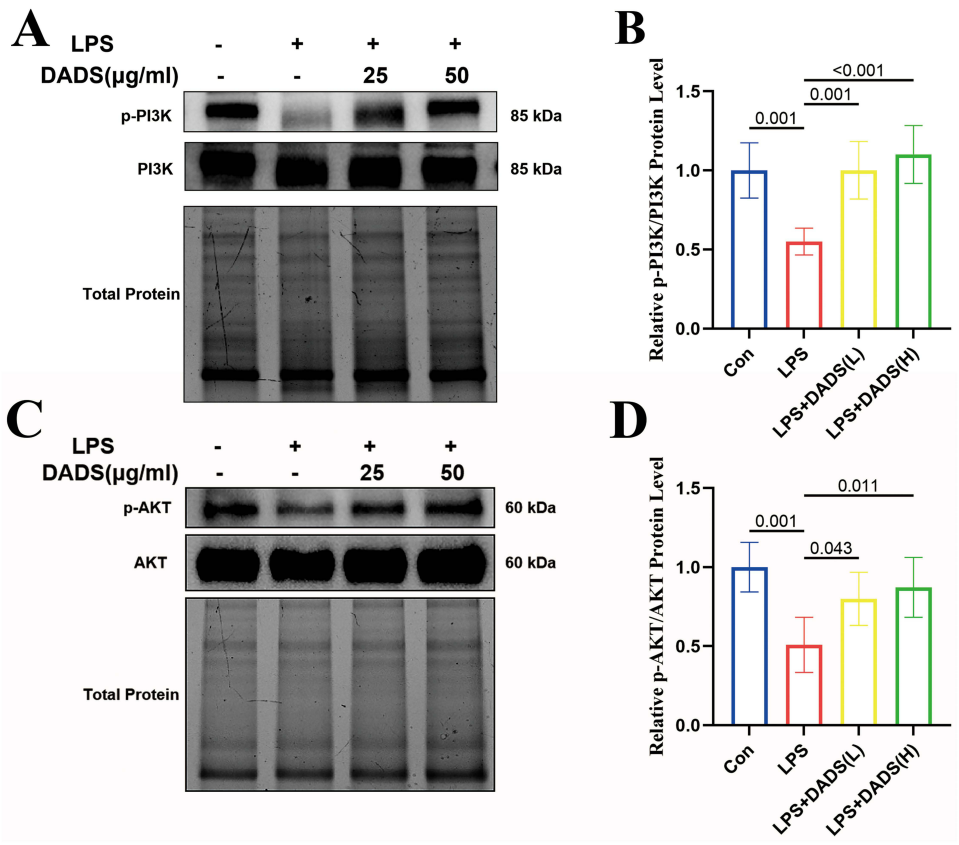

Figure 10 DADS activates the PI3K/AKT signaling pathway. (**A**–**D**) Representative images reflecting the expression levels of p-PI3K, PI3K, p-AKT, and AKT, along with their quantification, with total protein serving as a loading control. Statistical analysis was performed using one-way ANOVA. Data are presented as mean ± SD, n = 5 independent biological replicates per group. Exact P values for pairwise comparisons are shown above the horizontal lines; P < 0.001 denotes values below three-decimal precision.

Discussion

IBL is a common pathological process present in various inflammatory diseases. These diseases can manifest throughout the body, affecting systems such as the musculoskeletal system (eg., rheumatoid arthritis), the gastrointestinal tract (eg., inflammatory bowel disease), the oral cavity (eg., periodontitis), and the respiratory system (eg., cystic fibrosis).[1] The IBL process is marked by the participation of different inflammatory mediators that hinder bone formation by osteoblasts derived from BMSCs and boost bone resorption by osteoclasts through several signaling pathways, thereby disrupting bone homeostasis.[37,38] In situations of inflammation, the release of proinflammatory cytokines can inhibit the differentiation of osteoblasts, as supported by many studies.[39–42] TNF-α, for example, has been found to hinder osteoblast differentiation by activating the stress-activated protein kinase/c-Jun N-terminal kinase pathway.[43] Due to its considerable effect on patients, IBL is being acknowledged more and more as a major global public health issue that requires immediate attention.

Evidence suggests that DADS exhibit considerable anti-inflammatory and antioxidant qualities.[44] For example, studies have found that in cigarette smoke-induced mouse emphysema models, DADS treatment can restore the activity of key antioxidant enzymes such as SOD and GST in lung tissues, reduce the number of airway leukocyte infiltrations in mice, thereby alleviating lung tissue inflammation.[45] Furthermore, DADS has been shown to improve impaired chondrogenesis in human adipose-derived mesenchymal stem cells impacted by IL-1β/NF-κB by decreasing reactive oxygen species and boosting antioxidant enzyme activity.[27] Our earlier investigations also revealed that DADS has the potential to prevent osteoclastogenesis through the NF-κB/NFATc1 signaling pathway, thus alleviating LPS-induced inflammatory bone resorption in mouse calvaria with local treatment.[29]

In this study, μ-CT analysis of the right femur and Von Kossa staining of the lumbar vertebrae indicated that DADS prevented bone loss, when using the mouse IBL model in vivo. In toluidine blue staining of the right femur, staining

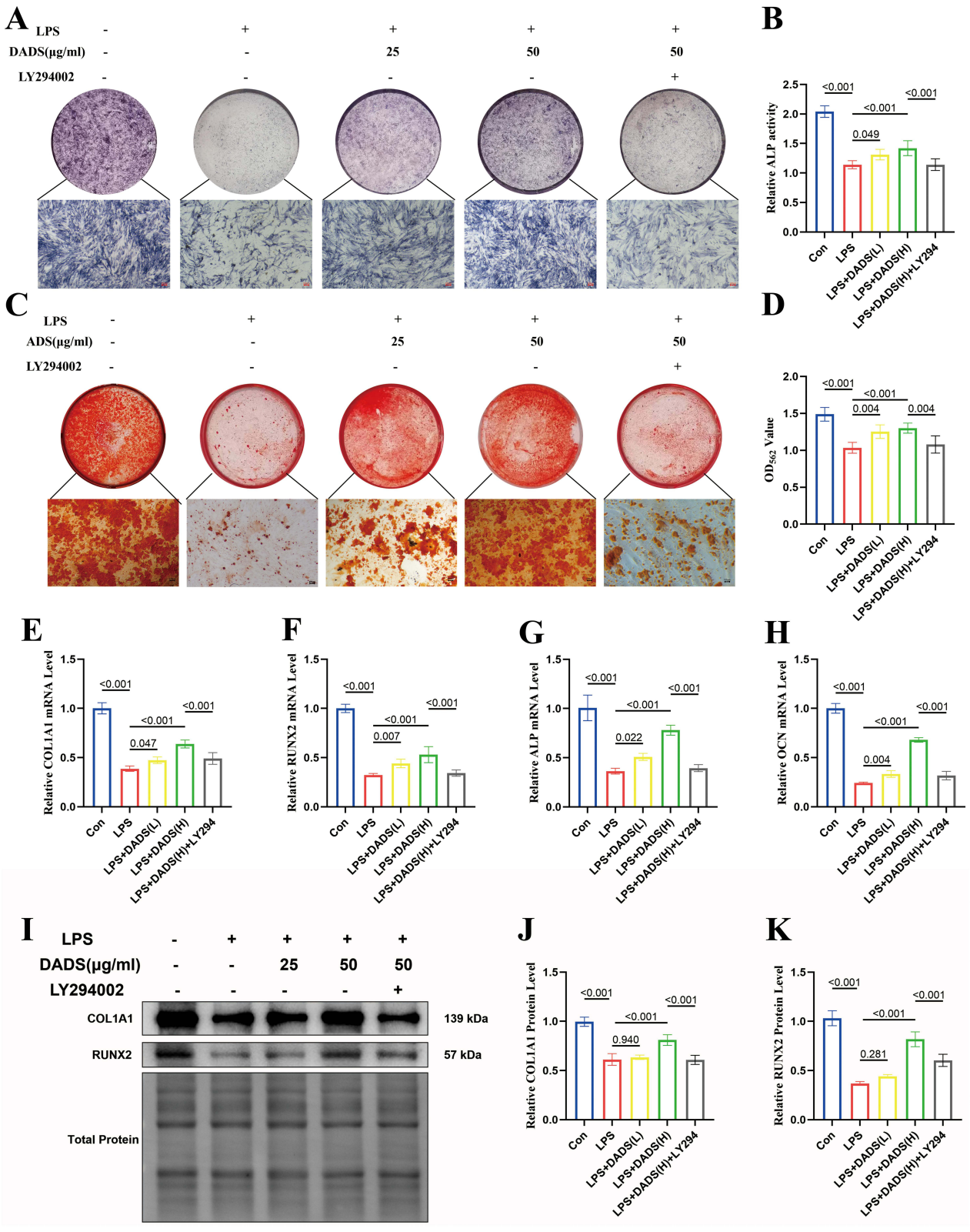

Figure 11 DADS rescues LPS-induced inhibition of osteogenic differentiation by activating the PI3K/AKT signaling pathway. (**A**) Representative images of ALP staining (scale bar = 100 μm). (**B**) ALP activity evaluation after 7 days of osteogenic induction. (**C**) Representative images of Alizarin Red staining after 14 days of osteogenic induction (scale bar = 100 μm). (**D**) Quantitative assessment of the calcium deposition in (**C**). (**E–H**) The expression of osteogenic-specific genes COL1A1, RUNX2, ALP, and OCN after 7 days of osteogenic induction. (**I–K**) Western blot and quantitative analysis of the levels of osteogenic markers COL1A1 and RUNX2 after 7 days of osteogenic induction, with total protein serving as a loading control. Statistical analysis was performed using one-way ANOVA. Data are presented as mean ± SD, n = 5 independent biological replicates per group. Exact P values for pairwise comparisons are shown above the horizontal lines; P < 0.001 denotes values below three-decimal precision.

https://doi.org/10.2147/DDDT.S590959

intensity and the Ob.S/BS ratio were both significantly increased. Furthermore, a considerable increase in the markers of osteogenic differentiation, COL1A1 and RUNX2. These results imply that DADS can improve osteogenic differentiation in IBL. Additionally, TRAP staining of the femur in this study demonstrated that DADS also inhibited osteoclast activity. This finding suggests that DADS may possess a dual regulatory effect, and the suppression of osteoclasts could be part of DADS' overall bone-protective mechanism, although this specific mechanism was not the primary focus of the current study. In addition, numerous in vitro assays, including ALP activity, Alizarin Red staining, immunofluorescence, qRT-PCR, and Western blot, were conducted to study the impact of DADS on reversal of LPS-induced inhibition of osteogenic differentiation. It was ultimately confirmed that DADS could significantly reverse the inhibitory effect of LPS on the osteogenic differentiation process.

To examine the effect of DADS on inflammatory response in IBL mice, we further measured the spleen index of mice, detected the levels of inflammatory factors IL-6, IL-1β, and TNF-α in serum by ELISA, and observed the expression level of inflammatory factors in the right femur by immunohistochemical staining. These results collectively indicate that DADS can downregulate the inflammatory response in IBL mice. DADS can also reduce the levels of COX-2 and inflammatory factors in LPS-induced BMSCs, as confirmed by qPCR and Western blot. The PTGS2 gene gives rise to COX-2, a vital enzyme in the inflammatory process. This enzyme is vital for the synthesis of prostaglandins and other eicosanoids, which are essential in mediating inflammation.[46] COX-2 is rapidly upregulated when exposed to inflammatory stimuli like LPS, cytokines, and oxidative stress, which boosts inflammatory signals and tissue injury.[47] In IBL, prostaglandin E2 (PGE2) generated by COX-2 is vital in tilting the balance of bone, as it prevents osteogenic differentiation while also being closely associated with inflammatory bone resorption.[47] COX-2's activity can be inhibited by NSAIDs.44 These non-steroidal anti-inflammatory drugs can reduce inflammation and pain against diseases like rheumatoid arthritis.[48] However, the use of COX-2 inhibitors is limited due to their cardiovascular side effects, which are linked to the inhibition of cardioprotective prostaglandins.[49]

We then studied the possible targets and the mechanism of DADS for the treatment of IBL through promoting osteogenic differentiation via network pharmacology, a methodology that is used to study the multi-target and multi-pathway synergistic mechanisms of drugs.[50] Given this method, we were able to determine that DADS could treat IBL through various targets and pathways, especially PTGS2 and the PI3K/AKT signaling pathway. To further investigate the mechanism by which DADS reverses the LPS-induced inhibition of osteogenic differentiation in BMSCs, transcriptome sequencing analysis was performed in the study. The results confirmed that the PI3K/AKT signaling pathway is involved in the therapeutic effects of DADS. The PI3K/AKT signaling pathway is known to regulate bone metabolism. Different experimental models showed that the pathway is crucial for osteogenic differentiation. For instance, studies revealed that interferon regulatory factor 1 enhances osteogenic marker expression and mineralized nodule formation via activating the PI3K/AKT pathway.[51] Furthermore, the PI3K/AKT signaling pathway facilitates fracture healing through its interaction with the Wnt/β-catenin pathway.[52] In addition, various natural compounds and bioactive molecules have also been demonstrated to promote osteogenesis through the PI3K/AKT pathway.[53–55] In the context of IBL, the activation of this pathway is also intricately linked to the osteogenic differentiation and mineralization.[56] Through Western blot analyses, we confirmed the essential role of the PI3K/AKT pathway in DADS-regulated osteogenic differentiation by demonstrating a notable reduction in phosphorylated PI3K/AKT levels following LPS treatment. Conversely, administering DADS led to a significant, dose-dependent rise in PI3K/AKT phosphorylation. Moreover, introducing a PI3K inhibitor greatly reduced the ability of DADS to promote osteogenic differentiation, indicating a strong link between the activation of the PI3K/AKT pathway and the enhancement of osteogenic differentiation induced by DADS. We further discussed the upstream regulatory events underlying DADS-mediated PI3K/AKT pathway activation. Considering that COX-2, a key target predicted by our network pharmacology analysis, was experimentally validated in our study, we postulated a potential functional interaction between COX-2 and the PI3K/AKT pathway. It is plausible that DADS indirectly modulates the PI3K/AKT pathway by regulating COX-2 expression and its downstream anti-inflammatory effects. However, this hypothesized crosstalk between COX-2 and the PI3K/AKT pathway requires further experimental verification in future studies.

The scientific importance of this study lies in discovering new therapeutic agents with the potential to combat IBL. DADS lower IBL by inhibiting the expression of COX-2 and triggering PI3K/AKT. In summary, the findings of this

study provide a theoretical basis for designing innovative drugs with both anti-inflammatory and bone formation activities, demonstrating the potential of DADS as a multifunctional drug for maintaining bone homeostasis. Although this study has deepened our understanding of the mechanism by which DADS protects IBL, there are still limitations. Firstly, this study did not investigate the effects of DADS on osteoclasts or their underlying mechanisms. While TRAP staining indicated phenotypic changes, specific in vitro experiments with osteoclast precursors and mechanistic studies are absent. In addition, we only evaluated DADS in an acute inflammation model, and its long-term efficacy and safety in chronic inflammatory conditions, such as rheumatoid arthritis, remain to be determined. These limitations highlight important directions for future research. Additionally, the positive control drug for the study was selected to be alendronate sodium rather than anti-inflammatory drugs like the COX-2 inhibitors. More studies are needed to determine the effectiveness of DADS and its therapeutic effects compared to anti-inflammatory drugs. Lastly, Our study did not evaluate the effect of DADS on osteogenic differentiation of BMSCs under normal conditions (ie., without inflammatory stimulation), thus we could not determine whether DADS actively promotes osteogenesis in steady-state conditions or merely reverses LPS-mediated inhibition. Future research will systematically assess the impact of DADS on osteogenic differentiation of BMSCs under normal conditions to gain a more comprehensive understanding of its therapeutic potential.

Conclusion

In conclusion, DADS demonstrates efficacy in mitigating inflammatory responses by downregulating inflammatory factors and COX-2 expression. Furthermore, it reverses the inhibitory effect of LPS on osteogenic differentiation and significantly ameliorates IBL in murine models. This mechanism is facilitated through the activation of the PI3K/AKT signaling pathway. As a potential therapeutic agent for IBL-related diseases, DADS has demonstrated promising preclinical evidence and warrants further investigation.

Data Sharing Statement

The data used and analyzed in this study are available from the corresponding author upon reasonable request.

Ethics Approval and Consent to Participate

All animal experiments were conducted at the Animal Experiment Center of Army Medical University in accordance with the "Regulations on the Management of Laboratory Animals of the People's Republic of China" and "Guidelines for the Ethical Review of Laboratory Animal Welfare". The study protocol was approved by the Animal Welfare and Ethics Committee of the University (Approval No. AMUWEC20257045).

Author Contributions

All authors made a significant contribution to the work reported, whether that is in the conception, study design, execution, acquisition of data, analysis and interpretation, or in all these areas; took part in drafting, revising or critically reviewing the article; gave final approval of the version to be published; have agreed on the journal to which the article has been submitted; and agree to be accountable for all aspects of the work.

Funding

This work was supported by the Chongqing Municipal Technology Innovation and Application Development of Sichuan-Chongqing Science and Technology Innovation Cooperation Program Project [grant numbers CSTB2024TIAD-CYKJCXX0036], the Chongqing Municipal Health Commission Major Project on Traditional Chinese Medicine [grant number 2023DBXM010], the Natural Science Foundation of Chongqing Municipality [grant number CSTB2024NSCQ-MSX0485], and the Sichuan Provincial Special Project for the Central Government Guiding Local Science and Technology Development [grant number 2023ZYD0288].

Disclosure

The authors declare no competing interests.

References

1. Redlich K, Smolen JS. Inflammatory bone loss: pathogenesis and therapeutic intervention. *Nat Rev Drug Discov*. 2012;11(3):234–250. doi:10.1038/nrd3669
2. Sapra L, Srivastava RK. Immunotherapy in the management of inflammatory bone loss in osteoporosis. *Adv Protein Chem Struct Biol*. 2025;144:461–491. doi:10.1016/bs.apcsb.2024.10.013
3. Zhao DY, McCann L, Hahn G, Hedrich CM. Chronic nonbacterial osteomyelitis (CNO) and chronic recurrent multifocal osteomyelitis (CRMO). *J Trans Autoimmun*. 2021;4:100095. doi:10.1016/j.jtauto.2021.100095
4. Wu JH, Bao QW, Wang SK, Zhou PY, Xu SG. Mechanisms of the masquelet technique to promote bone defect repair and its influencing factors. *Chin J Traumatol*. 2025;28(3):157–163. doi:10.1016/j.cjtee.2024.04.003
5. Choukroun E, Parnot M, Surmenian J, et al. Bone formation and maintenance in oral surgery: the decisive role of the immune system—a narrative review of mechanisms and solutions. *Bioengineering*. 2024;11(2):191. doi:10.3390/bioengineering11020191
6. Olaniyan MF, Muhibi MA, Olaniyan TB. Oxidative stress and inflammatory response interplay. *J Prev Diagn Treat Strateg Med*. 2023;2(2):94–100. doi:10.4103/jpdtsm.jpdtsm_73_23
7. Hu W, Yang G, Ao L, et al. NINJ1 impairs the anti-inflammatory function of hUC-MSCs with synergistic IFN-γ and TNF-α stimulation. *Chin J Traumatol*. 2025;28(4):276–287. doi:10.1016/j.cjtee.2025.04.003
8. Thomas MV, Puleo DA. Infection, inflammation, and bone regeneration: a paradoxical relationship. *J Dent Res*. 2011;90(9):1052–1061. doi:10.1177/0022034510393967
9. Sharma K, Kumar S, Prakash R, et al. Chebulinic acid alleviates LPS-induced inflammatory bone loss by targeting the crosstalk between reactive oxygen species/NFκB signaling in osteoblast cells. *Free Radic Biol Med*. 2023;194:99–113. doi:10.1016/j.freeradbiomed.2022.11.026
10. Xiao J, Han Q, Yu Z, et al. Morroniside inhibits inflammatory bone loss through the TRAF6-mediated NF-κB/MAPK signalling pathway. *Pharmaceuticals*. 2023;16(10):1438. doi:10.3390/ph16101438
11. Yu X, Quan J, Long W, et al. LL-37 inhibits LPS-induced inflammation and stimulates the osteogenic differentiation of BMSCs via P2X7 receptor and MAPK signaling pathway. *Exp Cell Res*. 2018;372(2):178–187. doi:10.1016/j.yexcr.2018.09.024
12. Lu YC, Yeh WC, Ohashi PS. LPS/TLR4 signal transduction pathway. *Cytokine*. 2008;42(2):145–151. doi:10.1016/j.cyto.2008.01.006
13. Zamyatina A, Heine H. Lipopolysaccharide recognition in the crossroads of TLR4 and Caspase-4/11 mediated inflammatory pathways. *Front Immunol*. 2020;11:585146. doi:10.3389/fimmu.2020.585146
14. Sapra L, Saini C, Sharma S, et al. Targeting the osteoclastogenic cytokine IL-9 as a novel immunotherapeutic strategy in mitigating inflammatory bone loss in post-menopausal osteoporosis. *JBMR Plus*. 2024;8(11):ziae120. doi:10.1093/jbmrpl/ziae120
15. Omata Y, Frech M, Lucas S, et al. Type 2 innate lymphoid cells inhibit the differentiation of osteoclasts and protect from ovariectomy-induced bone loss. *Bone*. 2020;136:115335. doi:10.1016/j.bone.2020.115335
16. Sampei C, Kato K, Arasaki Y, et al. *Gprc5a* is a novel parathyroid hormone-inducible gene and negatively regulates osteoblast proliferation and differentiation. *J Cell Physiol*. 2024;239(8):e31297. doi:10.1002/jcp.31297
17. Javinani A, Aghaei Meybodi HR, Kavosi H. Extremely elevated serum alkaline phosphatase level upon treatment with teriparatide: a case report. *J Med Case Rep*. 2020;14(1):87. doi:10.1186/s13256-020-02416-7
18. Subbiah V, Madsen VS, Raymond AK, Benjamin RS, Ludwig JA. Of mice and men: divergent risks of teriparatide-induced osteosarcoma. *Osteoporos Int*. 2010;21(6):1041–1045. doi:10.1007/s00198-009-1004-0
19. Gogakos AI, Anastasilakis AD. Current and emerging bone resorption inhibitors for the treatment of osteoporosis. *Expert Opin Pharmacother*. 2025;26(3):265–278. doi:10.1080/14656566.2025.2451741
20. Yun HM, Ban JO, Park KR, et al. Potential therapeutic effects of functionally active compounds isolated from garlic. *Pharmacol Ther*. 2014;142(2):183–195. doi:10.1016/j.pharmthera.2013.12.005
21. De Greef D, Barton EM, Sandberg EN, et al. Anticancer potential of garlic and its bioactive constituents: a systematic and comprehensive review. *Semin Cancer Biol*. 2021;73:219–264. doi:10.1016/j.semcancer.2020.11.020
22. Nakamoto M, Kunimura K, Suzuki JI, Kodera Y. Antimicrobial properties of hydrophobic compounds in garlic: allicin, vinyldithiin, ajoene and diallyl polysulfides. *Exp Ther Med*. 2020;19(2):1550–1553. doi:10.3892/etm.2019.8388
23. Farhat Z, Scheving T, Aga DS, et al. Antioxidant and antiproliferative activities of several garlic forms. *Nutrients*. 2023;15(19):4099. doi:10.3390/nu15194099
24. Wang X, Liu Y, Dong X, et al. peu-MIR2916-p3-enriched garlic exosomes ameliorate murine colitis by reshaping gut microbiota, especially by boosting the anti-colitic Bacteroides thetaiotaomicron. *Pharmacol Res*. 2024;200:107071. doi:10.1016/j.phrs.2024.107071
25. Sobenin IA, Myasoedova VA, Iltchuk MI, Zhang DW, Orekhov AN. Therapeutic effects of garlic in cardiovascular atherosclerotic disease. *Chin J Nat Med*. 2019;17(10):721–728. doi:10.1016/S1875-5364(19)30088-3
26. Liu J, Li W, Bian Y, et al. Garlic-derived exosomes regulate PFKFB3 expression to relieve liver dysfunction in high-fat diet-fed mice via macrophage-hepatocyte crosstalk. *Phytomedicine*. 2023;112:154679. doi:10.1016/j.phymed.2023.154679
27. Bahrampour Juybari K, Kamarul T, Najafi M, Jafari D, Sharifi AM. Restoring the IL-1β/NF-κB-induced impaired chondrogenesis by diallyl disulfide in human adipose-derived mesenchymal stem cells via attenuation of reactive oxygen species and elevation of antioxidant enzymes. *Cell Tissue Res*. 2018;373(2):407–419. doi:10.1007/s00441-018-2825-y
28. Qian YQ, Feng ZH, Li XB, et al. Downregulating PI3K/Akt/NF-κB signaling with allicin for ameliorating the progression of osteoarthritis: in vitro and vivo studies. *Food Funct*. 2018;9(9):4865–4875. doi:10.1039/c8fo01095a
29. Yang J, Tang R, Yi J, et al. Diallyl disulfide alleviates inflammatory osteolysis by suppressing osteoclastogenesis *via* NF-κB–NFATc1 signal pathway. *FASEB J*. 2019;33(6):7261–7273. doi:10.1096/fj.201802172R
30. Long F. Building strong bones: molecular regulation of the osteoblast lineage. *Nat Rev Mol Cell Biol*. 2012;13(1):27–38. doi:10.1038/nrm3254
31. Wang J, Zhang Y, Xu X, et al. ASP2-1, a polysaccharide from Acorus tatarinowii Schott, inhibits osteoclastogenesis via modulation of NFATc1 and attenuates LPS-induced bone loss in mice. *Int J Biol Macromol*. 2020;165:2219–2230. doi:10.1016/j.ijbiomac.2020.10.077
32. Kwak SC, Baek JM, Lee CH, Yoon KH, Lee MS, Kim JY. Umbelliferone prevents lipopolysaccharide-induced bone loss and suppresses RANKL-induced osteoclastogenesis by attenuating Akt-c-Fos-NFATc1 signaling. *Int J Biol Sci*. 2019;15(11):2427–2437. doi:10.7150/ijbs.28609

33. Tan L, Miao Z, Zhao Y, et al. Dual regulation of phaseol on osteoclast formation and osteoblast differentiation by targeting TAK1 kinase for osteoporosis treatment. *J Adv Res*. 2024:S2090123224005654. doi:10.1016/j.jare.2024.12.009
34. Wang W, Wang Q, Li W, et al. Targeting APJ drives BNIP3-PINK1-PARKIN induced mitophagy and improves systemic inflammatory bone loss. *J Adv Res*. 2024:S2090123224006118. doi:10.1016/j.jare.2024.12.033
35. Lin Z, Gu Y, Liu Y, et al. Melatonin attenuates inflammatory bone loss by alleviating mitophagy and lactate production. *Apoptosis*. 2025;30 (5–6):1351–1371. doi:10.1007/s10495-025-02096-y
36. Li SD, Xing W, Wang SC, et al. Fibulin2: a negative regulator of BMSC osteogenic differentiation in infected bone fracture healing. *Exp Mol Med*. 2023;55(2):443–456. doi:10.1038/s12276-023-00942-0
37. Le Goff B, Bouvard B, Lequerre T, et al. Implication of IL-17 in bone loss and structural damage in inflammatory rheumatic diseases. *Mediators Inflamm*. 2019;2019:8659302. doi:10.1155/2019/8659302
38. Amarasekara DS, Yu J, Rho J. Bone loss triggered by the cytokine network in inflammatory autoimmune diseases. *J Immunol Res*. 2015;2015:832127. doi:10.1155/2015/832127
39. Zaidi M. Skeletal remodeling in health and disease. *Nat Med*. 2007;13(7):791–801. doi:10.1038/nm1593
40. Kaneki H, Guo R, Chen D, et al. Tumor necrosis factor promotes Runx2 degradation through up-regulation of Smurf1 and Smurf2 in osteoblasts. *J Biol Chem*. 2006;281(7):4326–4333. doi:10.1074/jbc.M509430200
41. Hughes FJ, Howells GL. Interleukin-11 inhibits bone formation in vitro. *Calcif Tissue Int*. 1993;53(5):362–364. doi:10.1007/BF01351844
42. Krum SA, Chang J, Miranda-Carboni G, Wang CY. Novel functions for NFκB: inhibition of bone formation. *Nat Rev Rheumatol*. 2010;6 (10):607–611. doi:10.1038/nrrheum.2010.133
43. Mukai T, Otsuka F, Otani H, et al. TNF-alpha inhibits BMP-induced osteoblast differentiation through activating SAPK/JNK signaling. *Biochem Biophys Res Commun*. 2007;356(4):1004–1010. doi:10.1016/j.bbrc.2007.03.099
44. Ho SC, Su MS. Evaluating the anti-neuroinflammatory capacity of raw and steamed garlic as well as five organosulfur compounds. *Molecules*. 2014;19(11):17697–17714. doi:10.3390/molecules191117697
45. Cardoso ADOP, e Silva CP, Dos Anjos FDF, et al. Diallyl disulfide prevents cigarette smoke-induced emphysema in mice. *Pulm Pharmacol Ther*. 2021;69:102053. doi:10.1016/j.pupt.2021.102053
46. Vane JR, Bakhle YS, Botting RM. Cyclooxygenases 1 and 2. *Annu Rev Pharmacol Toxicol*. 1998;38(1):97–120. doi:10.1146/annurev.pharmtox.38.1.97
47. Coon D, Gulati A, Cowan C, He J. The role of cyclooxygenase-2 (COX-2) in inflammatory bone resorption. *J Endod*. 2007;33(4):432–436. doi:10.1016/j.joen.2006.12.001
48. Lee SJ, Park MK, Shin DS, Chun MH. Variability of the drug response to nonsteroidal anti-inflammatory drugs according to cyclooxygenase-2 genetic polymorphism. *Drug Des Devel Ther*. 2017;11:2727–2736. doi:10.2147/DDDT.S143807
49. Ricciotti E, Castro C, Tang SY, et al. Cyclooxygenase-2, asymmetric dimethylarginine, and the cardiovascular hazard from nonsteroidal anti-inflammatory drugs. *Circulation*. 2018;138(21):2367–2378. doi:10.1161/CIRCULATIONAHA.118.033540
50. Zhao L, Zhang H, Li N, et al. Network pharmacology, a promising approach to reveal the pharmacology mechanism of Chinese medicine formula. *J Ethnopharmacol*. 2023;309:116306. doi:10.1016/j.jep.2023.116306
51. Hu M, Wei E, Wu L, et al. IRF1 regulates apoptosis and osteogenic differentiation of bone marrow mesenchymal stem cells and ameliorates osteoporosis by activating the PI3K/AKT signaling pathway. *J Adv Res*. 2025:S2090–1232(25)00933–6. doi:10.1016/j.jare.2025.11.037
52. Dong J, Xu X, Zhang Q, Yuan Z, Tan B. The PI3K/AKT pathway promotes fracture healing through its crosstalk with wnt/β-catenin. *Exp Cell Res*. 2020;394(1):112137. doi:10.1016/j.yexcr.2020.112137
53. Song Y, Hu J, Yang P, et al. Astragaloside IV promotes osteogenic differentiation of periodontal ligament stem cells via activating PI3K/AKT/eNOS/NO signaling pathway: in vitro and in vivo study. *DDDT*. 2025;19:6073–6088. doi:10.2147/DDDT.S514682
54. Jiang Z, Deng L, Li M, Alonge E, Wang Y, Wang Y. Ginsenoside Rg1 modulates PI3K/AKT pathway for enhanced osteogenesis via GPER. *Phytomedicine*. 2024;124:155284. doi:10.1016/j.phymed.2023.155284
55. Chai S, Yang Y, Wei L, et al. Luteolin rescues postmenopausal osteoporosis elicited by OVX through alleviating osteoblast pyroptosis via activating PI3K-AKT signaling. *Phytomedicine*. 2024;128:155516. doi:10.1016/j.phymed.2024.155516
56. Li J, Mai J, Zhang M, et al. Myricitrin promotes osteogenesis and prevents ovariectomy bone mass loss via the PI3K/AKT signalling pathway. *J Cell Biochem*. 2023;124(8):1155–1172. doi:10.1002/jcb.30439